Int. J. Electron. Commun. (AEÜ) 137 (2021) 153798

Contents lists available at ScienceDirect

International Journal of Electronics and Communications

journal homepage: www.elsevier.com/locate/aeue

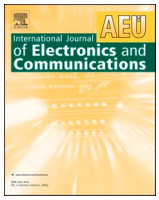

Regular paper

# Additive manufacturing of a compact Ku-band orthomode transducer

José R. Montejo-Garai [a,*], Jorge A. Ruiz-Cruz [b], Jesús M. Rebollar [a]

[a] Grupo de Electromagnetismo Aplicado, Information Processing and Telecommunications Center, Universidad Politécnica de Madrid, Madrid, Spain
[b] Escuela Politécnica Superior, Universidad Autónoma de Madrid, Madrid, Spain

ARTICLE INFO

*Keywords:*
Orthomode transducer
OMT
Orthogonal linear polarizations
Additive manufacturing
AM
Selective Laser Melting
SLM

ABSTRACT

This work presents a compact ortho-mode transducer (OMT) built by additive manufacturing in a single-block, reducing the number of parts and flanges and improving the losses and power handling capability. The single-block approach also reduces potential passive intermodulation issues since the number of interfaces between parts is minimized. The presented OMT is based on the T-junction topology, with a short-circuited common circular waveguide where the two rectangular waveguides ports are attached. Both ports are arranged in opposite direction to maintain a symmetry plane for the whole structure in order to obtain a high isolation. Specific matching elements are introduced for each polarization to route the orthogonal modes to the common waveguide. The device is built by Selective Laser Melting (SLM), which imposes a set of specific mechanical restrictions to the 3D model of the OMT. The proposed design incorporates those restrictions, simplifying the geometry of the OMT as much as possible (especially the routing elements) to simplify the manufacturing. After this process, the experimental results show an OMT working in the band from 13.4 to 15.6 GHz (15.2%) with a return loss level higher than 20 dB for both polarizations, insertion loss lower than 0.18 dB and isolation between polarizations better than 45 dB. The OMT has also been tested in radiation connected to a reference horn, measuring a cross-polarization lower than −45 dB. This experimental performance shows that the proposed combination of compact design with single-block SLM manufacturing provides tested results similar to those obtained by high-accuracy milling or spark erosion suitable for satellite applications.

## 1. Introduction

Ortho-mode transducers (OMTs) are crucial devices in high transmission satellite and radio communication systems, where dual-polarized antenna feed subsystems need to separate or combine signals with different orthogonal polarizations [1–5]. Radioastronomy is another specific field where OMTs play a decisive role in polarization discrimination [6–10]. Very challenging electric performances are usually imposed to this type of devices in terms of bandwidth, return loss, insertion loss, isolation and cross-polarization level, especially for satellite systems. In fact, the cross-polarization level is one of the most challenging requirements, because it depends on two factors: the dimensional accuracy to manufacture the device and the symmetry planes found in its 3D topology [11].

Besides, compact structure, high power handling, low mass, easy integration and low cost, are other expected requisites for OMTs in the new high throughput satellites (HTS) with multi-beam antennas [12], which increase significantly the efficiency of the traditional fixed service satellites. Another application area for OMTs is the Low Earth Orbit (LEO) mega-constellations [13], where mass production requires simple and compact structures without compromising the electrical performance.

At the same time, the application of the Additive Manufacturing (AM) techniques in microwave engineering has been continuously growing [14–19], and waveguide technology has followed the same trend. Powder bed fusion processes like Selective Laser Melting (SLM) [20] or diffusion bonding [21,22] allow to manufacture all-metal devices. Considering the potential benefits regarding to the mass reduction, cost, integration, and design flexibility, its vertiginous development affects a large number of components of the front-end of communications system, and the OMTs are clearly benefiting of these developments [23–26], leading to very compact designs carried out with 3D-printing approaches [27–31].

Therefore, the goal of this work is twofold. Firstly, to design a Ku-band OMT with a very simple and compact geometry taking into account the mechanical restrictions of the intended additive

* Corresponding author.
*E-mail addresses:* joseramon.montejo@upm.es (J.R. Montejo-Garai), jorge.ruizcruz@uam.es (J.A. Ruiz-Cruz), jmrm@etc.upm.es (J.M. Rebollar).

https://doi.org/10.1016/j.aeue.2021.153798
Received 14 March 2021; Accepted 5 May 2021
Available online 11 May 2021

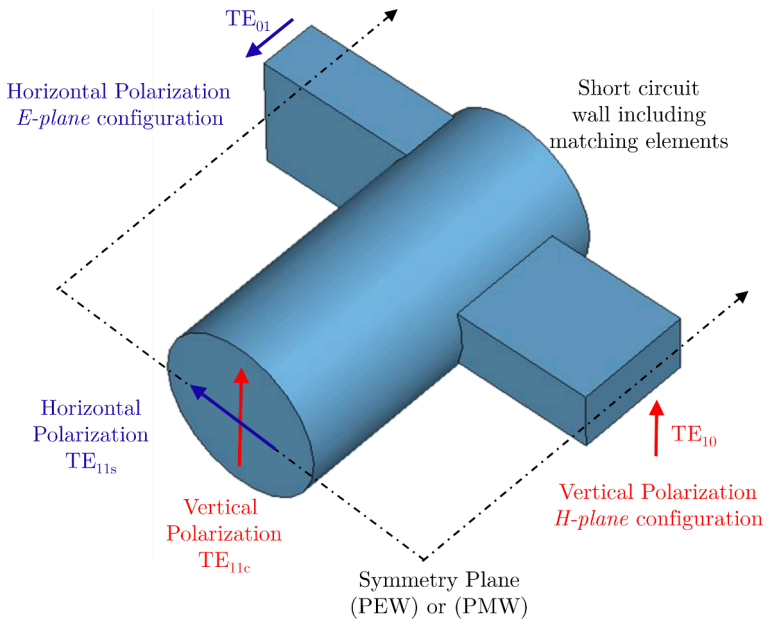


**Fig. 1.** General scheme of the compact OMT based on a T-junction with the common port at the circular waveguide and the dedicated rectangular waveguide ports attached at opposite sides of the cylinder. The routing of the vertical polarization is done in *H-plane* configuration, while for the horizontal polarization is *E-plane*. Each case leads to a symmetry plane with either Perfect Electric or Magnetic Wall (PEW/PMW) boundary condition.

manufacturing, in particular by SLM with aluminum powder alloy. Secondly, to fabricate the device in a single-block to reduce losses, to improve power handling and to prevent PIM (Passive Inter Modulation) issues [18]. The presented results show that is possible to obtain excellent performances in return loss, insertion loss, isolation and cross-polarization, at the same level than those obtained by the classic Computer Numerical Control (CNC) milling for satellite applications.

The presented OMT, based on the T-junction topology is addressed using specific routing elements for each polarization designed ad hoc for easing the single-block manufacturing and leading to a very compact structure. For the same reason, the circular transformer integrated between the common port of the OMT and the antenna horn is limited to one section, with a careful control of the higher-order $TM_{01}$ mode, not always covered in detail in the technical literature. The experimental results, i.e., the return loss, the insertion loss and the isolation are measured for a single part and also for a back-to-back arrangement. These parameters, along with an additional accurate measurement of the cross-polar radiation pattern of the OMT connected with a reference horn, validate the proposed design, which will be also compared with other designs in the state of the art.

## 2. Design of the orthomode transducer

The OMT proposed in this work is based on a T-junction formed by a circular waveguide short-circuited at one end [1,32–34]. Two rectangular waveguides are connected close to the short-circuit of the common waveguide at opposed side walls, with a relative angle of 180°, as shown in Fig. 1. The structure presents a symmetry plane with Perfect Electric Wall (PEW) boundary condition for the vertical polarization, and Perfect Magnetic Wall (PMW) boundary condition for the horizontal polarization. This symmetry is exploited in the electromagnetic simulations to reduce the numerical effort analyzing only one half of the device, with either PEW or PMW.

The two *WR75* rectangular ports allocate the dedicated orthogonal linear vertical and horizontal polarizations in the $TE_{10}$ and $TE_{01}$ modes, respectively. The vertical polarization is routed between the dedicated rectangular port and the common circular port in *H-plane* configuration, while the horizontal polarization is routed in *E-plane* configuration. The $TE_{11c}$ ($TE_{11s}$) mode at the circular waveguide is generated by the $TE_{10}$ ($TE_{01}$) mode at the dedicated rectangular port. Depending on the radius of the circular waveguide, the higher-order modes $TM_{01}$, $TE_{21c}$ and $TE_{21s}$ could also propagate because their cutoff frequencies may lie in the operation bandwidth from 13.4 to 15.6 GHz. Thus, a critical goal in this design is to minimize their generation when selecting the matching elements for each polarization, maintaining the symmetry plane of the structure.

The design process can be divided in three tasks, where two of them must be accomplished simultaneously: the design of the *H-plane* branch for the vertical polarization and the design of the *E-plane* branch port for the horizontal polarization. The third task is the design of the transformer between the circular waveguide of the T-junction and the circular waveguide of the horn antenna.

Since the T-junction maintains a symmetry plane across the center of the three waveguide ports as shown in Fig. 1, both polarizations are ideally uncoupled, i.e., the isolation between them is infinite in the ideal symmetric structure. Thus, the isolation parameter is not included in the initial design of the OMT, since full uncoupling is granted by the OMT topology. Nevertheless, unavoidable manufacturing tolerances always lead to a certain level of undesired coupling between orthogonal polarizations in tested OMTs, which will be in the order of 40 dB for accurate manufacturing at Ku-band.

The radius of the horn antenna that will be connected to the OMT is 9.675 mm, very close to the standard circular waveguide *IEC C109* (radius 9.75 mm). The cut-off frequencies of the propagating modes under the upper limit of the operation band (15.6 GHz) are 9.08 GHz for the $TE_{11c,s}$ modes, 11.85 GHz for the $TM_{01}$ mode, and 15.06 GHz for the $TE_{21c,s}$ modes. Therefore, the radius of the common circular waveguide is a key parameter in the design process to match both polarizations and to control the higher-order modes that will be under cutoff.

The design and optimization of the OMT is accomplished by means of the CST Microwave Studio[35]. Moreover, the limitations of the AM process are also considered at the initial design steps, including the limits for the minimum features that can be achieved with SLM, as it will be shown in the next subsections. This is very important for obtaining a successful experimental prototype.

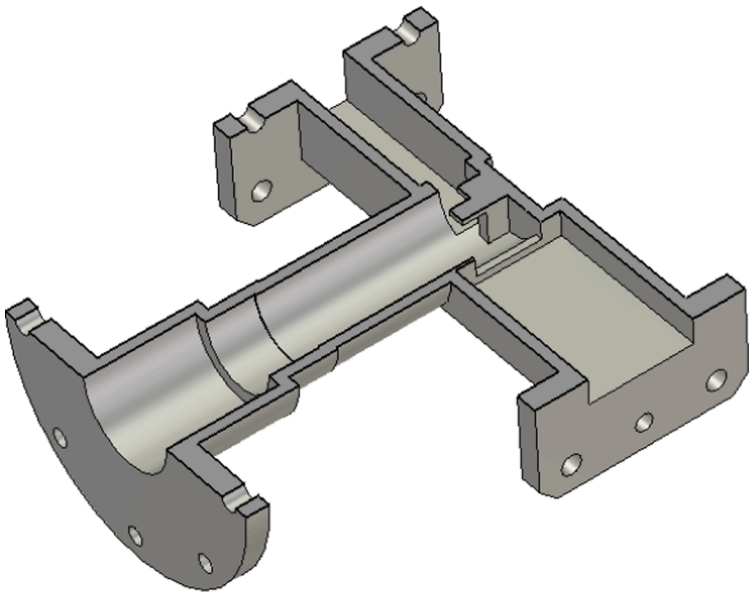

**Fig. 2.** 3D CAD of one half the OMT showing the inner parts; matching elements are placed at the short-circuit side of the circular cylinder and a single-section circular transformer is used at the common circular waveguide. Rectangular ports are WR75 (19.05 × 9.525 $mm^2$) and common circular port has a diameter of 19.35 mm.

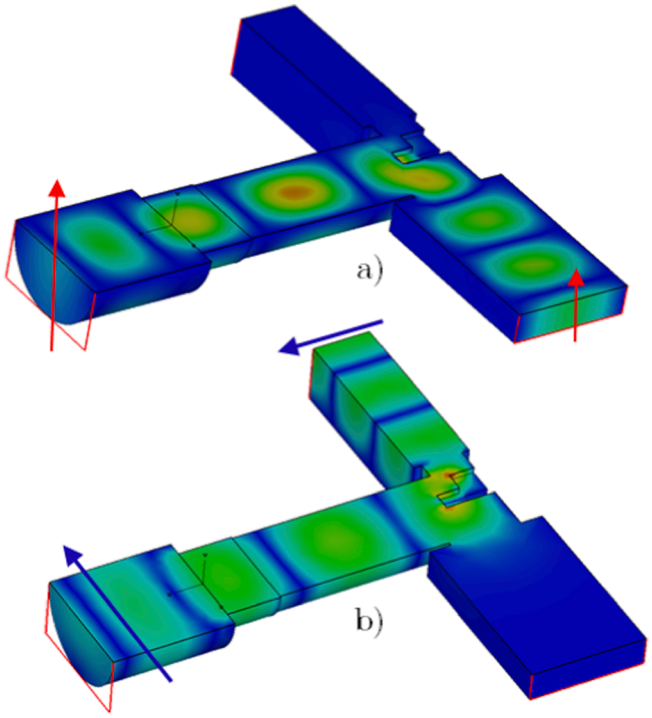


**Fig. 3.** a) Magnitude of the electric field when feeding the OMT through the *H-plane* port with the vertical polarization at center frequency of 14.5 (GHz). b) Magnitude of the electric field when feeding the OMT through the *E-plane* port with the horizontal polarization at center frequency of 14.5 (GHz).

### 2.1. H-plane branch for feeding the vertical polarization

The *H-plane* port feeds the vertical polarization. The first element to couple the rectangular $TE_{10}$ mode to the circular waveguide is a centered rectangular iris (Fig. 2) whose minimum thickness (0.5 mm) is limited by the AM process. The distance from the port to the short-circuited bottom wall is a key parameter in order to add in phase the reflected signal at the short-circuit and the region of the problem under cutoff. This can be seen in Fig. 3(a), which shows the magnitude of the electric field when feeding the OMT through the $TE_{10}$ at the port with the vertical polarization at center frequency of 14.5 (GHz). The Fig. 2 also helps to see that the branch for the dedicated horizontal polarization is under cutoff for PEW at the symmetry plane. A transverse ridge crossing the short-circuited end wall, with the same direction than the polarization, is added to ease the routing of the electromagnetic field towards the output. Since the symmetrical plane behaves like a PEW, for this polarization the only propagating mode in the circular waveguide is the $TE_{11c}$ mode.

### 2.2. E-plane branch for feeding the horizontal polarization

The *E-plane* port feeds the horizontal polarization. The first element to couple the rectangular $TE_{01}$ mode to the circular waveguide is a change in the height of the standard *WR*75 rectangular waveguide (Fig. 2). This change arises from the evolution of an initial centered iris during the optimization process. As in the case of the vertical polarization, the distance from the port to the short-circuited end wall is crucial for the matching. An *H-shape* pedestal (Fig. 2) is included as an stepped bend to route the electromagnetic field towards the output. With these matching elements, the symmetry plane is maintained and behaves like a PMW; in this case the two modes with lowest cutoff frequency are the $TE_{11s}$ and the $TM_{01}$ modes. Therefore, the radius of the circular common waveguide has to be lower than 7.35 mm to ensure that the cut-off frequency of the $TM_{01}$ mode is higher than 15.6 GHz.

It must be appointed that the optimization process to fulfill the return loss specification (20 dB theoretically for the band 13.4–14.6 GHz) takes into account both polarizations simultaneously. The cost function also controls the attenuation level of the $TM_{01}$ mode, which is only generated in the problem associated to the horizontal polarization. After the optimization with the exposed restrictions, the final value of the radius is 7.12 mm. Fig. 3(b) shows the magnitude of the electric field when feeding the OMT through this port at center frequency of 14.5 (GHz), showing the branch for the vertical polarization under cutoff.

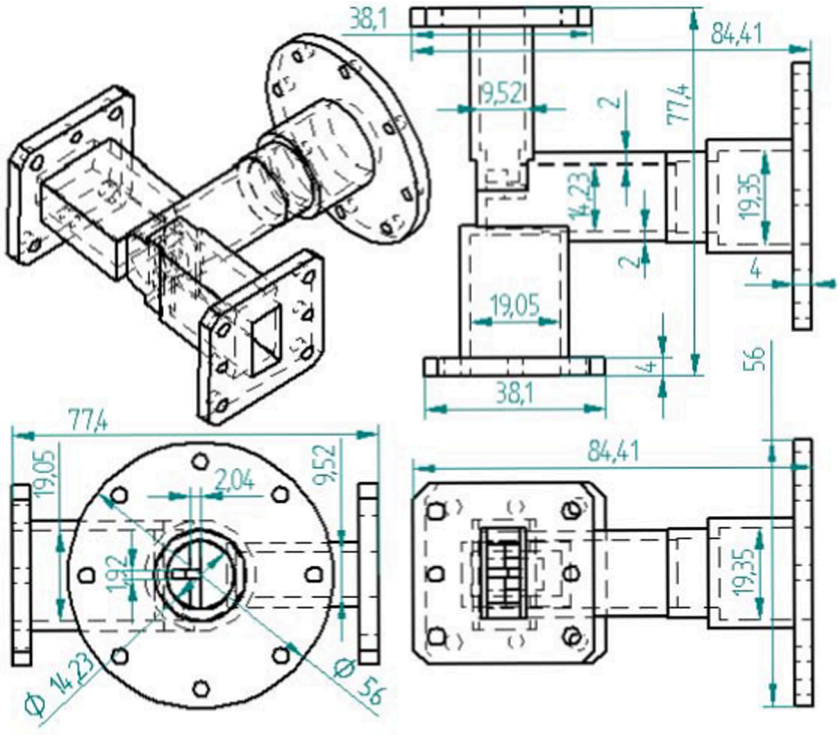


**Fig. 4.** CAD views for the single-block printing of the Ku-band OMT: 3D, side, top and bottom views. Main dimensions in mm.

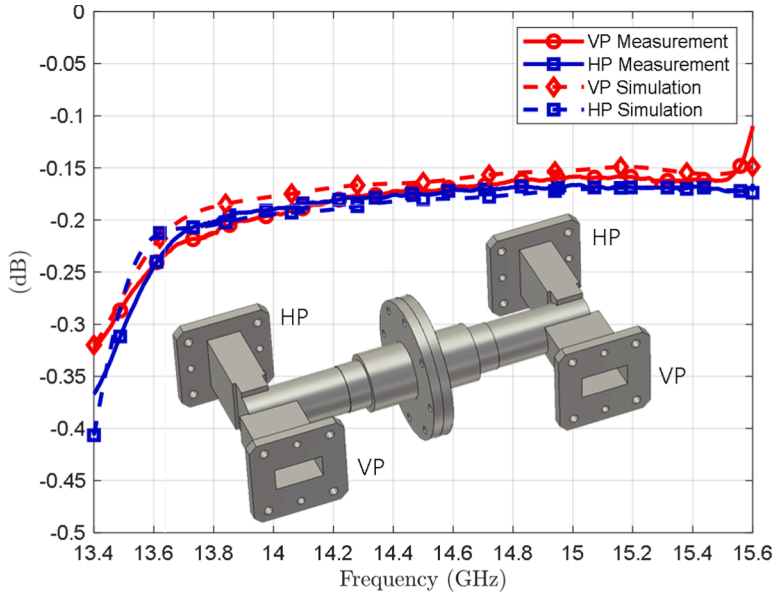


**Fig. 5.** Comparison of the insertion loss (S parameters) between the full-wave simulation of the two OMTs in back-to-back configuration and the measurements. This is done for both the vertical (VP) and the horizontal (HP) polarizations. An effective conductivity of $\sigma_{eff} = 3$ MS/m is considered for the simulation. A 3D CAD of the connected prototypes and the identification of the ports is shown in the inset.

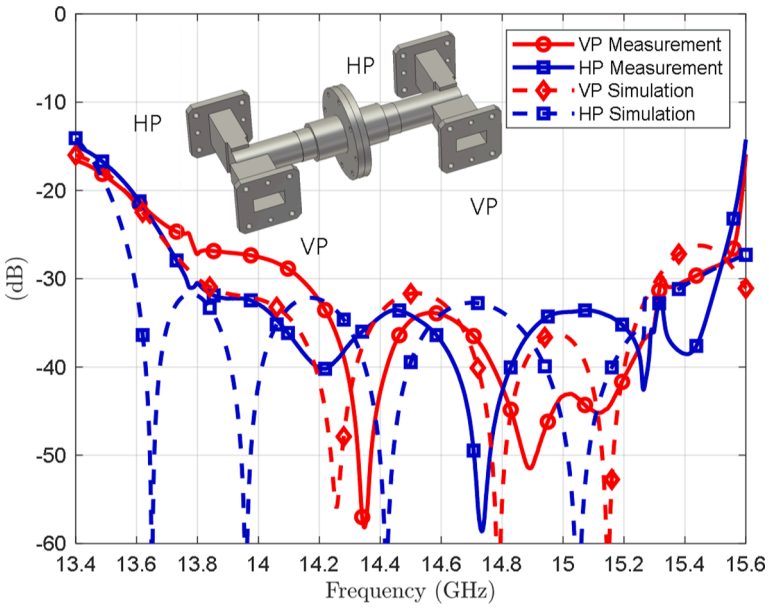


**Fig. 6.** Comparison of the return loss (S parameters) between the full-wave simulation of the two OMTs in back-to-back configuration and the measurements. This is done for both the vertical (VP) and the horizontal (HP) polarizations. An effective conductivity of $\sigma_{eff} = 3$ MS/m is considered for the simulation. A 3D CAD of the connected prototypes and the identification of the ports is shown in the inset.

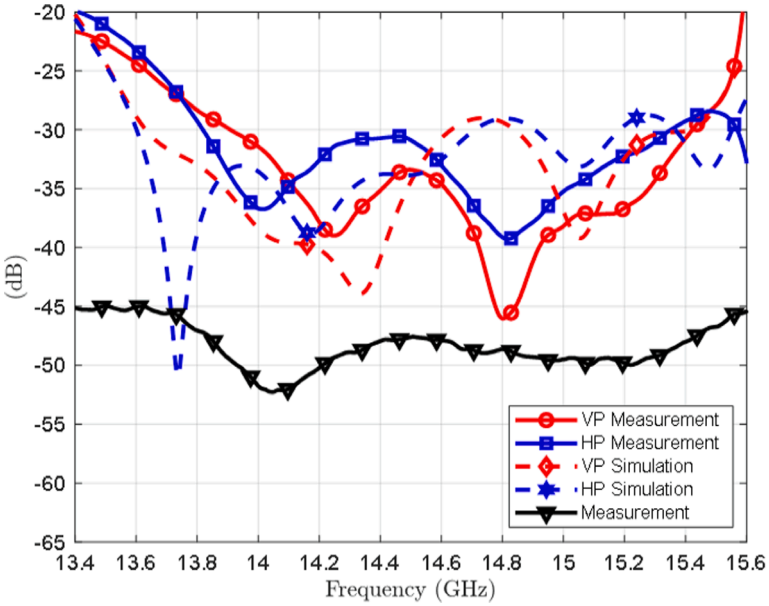


**Fig. 7.** Comparison of the return loss (S parameters) between the full-wave simulation of a single orthomode transducer and the measurement for the vertical and the horizontal polarization and measured isolation between polarizations (see setup in Fig. 8). An effective conductivity of $\sigma_{eff} = 3$ MS/m is considered for the simulation.

### 2.3. Circular waveguide transformer

Once the T-junction with the two ports has been designed, the last task is to add a transformer to connect the horn antenna (input radius of 9.675 mm) to the common circular waveguide (radius 7.12 mm). One section is enough to maintain the previously obtained matching level, keeping the level of the $TM_{01}$ mode under $-50$ dB.

As previously stated, the topology for the OMT, and all its inner parts and components, have been chosen considering the 3*D* printing process by SLM. The inner structure, whose simplicity is evident as can be seen in Fig. 2, has been carefully reviewed with the mechanic technologist to guarantee the experimental results. Fig. 4 shows the main draft views of the manufactured model, including the total external dimensions of the single-block device ($77.4 \times 84.4 \times 56$ mm$^3$) and the thickness of the SLM walls (2 mm). The inner part without reference planes has a size of $19.5 \times 50.1 \times 19.3$ mm$^3$.

## 3. Experimental results

With the aim of verifying the theoretical results, two equal devices have been printed by SLM technology using *AlSi*10*Mg* aluminum alloy powder. Each OMT is manufactured in a single-block.The typical achievable accuracy is $\pm 100$ μm, according to the authors' experience [36], since the fabrication accuracy is not provided by the supplier.

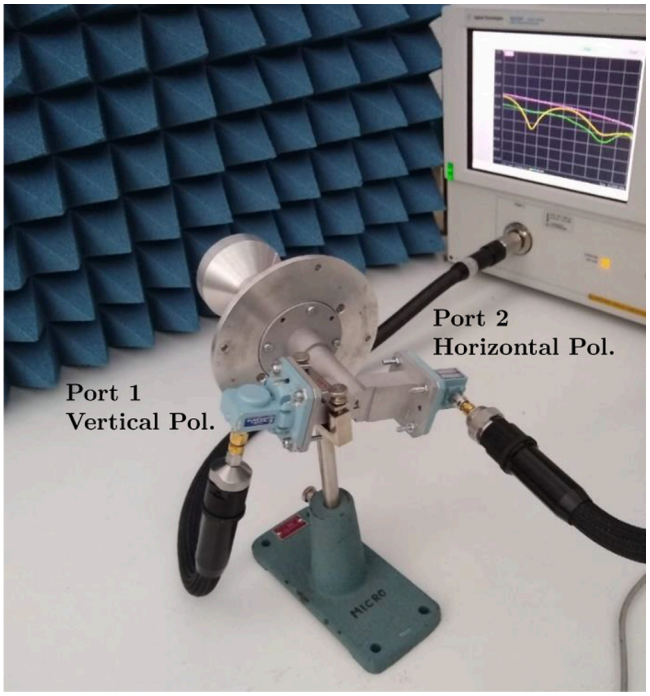


**Fig. 8.** Setup configuration for the measurement of the return loss of both polarizations and the isolation between ports. The common port is connected to a horn (with return loss level better than 35 dB) working as load and radiating towards the absorbent panel.

Both, the insertion loss and the return loss have been measured in a back-to-back configuration for the vertical and horizontal polarization, with the other ports loaded with high-accuracy matched loads. Besides, the return loss and the isolation of a single OMT have been also measured loading the common port with a conical horn whose return loss level was higher than 35 dB in the specified bandwidth.

Fig. 5 shows the comparison between the simulated insertion loss and the measurements, considering an effective conductivity for the aluminum $\sigma_{eff} = 3$ MS/m. Since the theoretical value of the aluminum alloy powder is not provided by the SLM external supplier, this effective parameter takes into account the roughness of the walls and the manufacturing process. As it can be observed, the agreement is very good. The highest value of the insertion loss for a single OMT is 0.18 dB for any of the two polarizations. Fig. 6 shows the comparison of the simulated return loss and the measurements, considering the same effective conductivity for the aluminum as previously.

The experimental results considering a single OMT are shown in Fig. 7, where the measured return loss for both polarizations is lower than 20 dB. The measured isolation is better than 45 dB, an excellent value in the state of the art for this type of compact asymmetric OMTs. It is emphasized that this value implies a very good accuracy in the manufacturing for preserving the OMT symmetry (the two polarizations would be perfectly isolated for the ideal symmetric OMT). This is a very important aspect to highlight since the OMT has been 3D printed by SLM in a single-block. A photograph of the measurement setup in Fig. 8 shows the configuration for the above measurements with the antenna horn connected to the OMT and working as the load for the common port, radiating towards the absorbent panel.

The previous OMT characterization is further validated with radiation patterns measured in the anechoic chamber at the center frequency of 14.5 GHz. Fig. 9 shows the measured normalized co-polar (CP) and cross-polar radiation patterns for the vertical polarization. Fig. 10 shows the equivalent patterns for the horizontal polarization. Finally, Fig. 11 shows the measured results for the cross-polarization level for $\theta = 0°$, $\phi = 0°$. A *gold standard* for the antenna horn lower than $-55$ dB in the whole operation band is taken as reference. The experimental results show that the cross-polarization level of the OMT is lower than $-45$ dB for both polarizations, confirming the good accuracy in the manufacturing, which has been possible thanks to the simplification of the OMT structure to exploit the SLM technology.

A comparison of different OMTs is shown in Table 1. It compares the performance of several state of the art works in return loss, insertion loss, and frequency bands. The table is limited to similar OMTs with only one symmetry plane, and dimensions are included when available. The table shows how the SLM technology can be competitive for future designs.

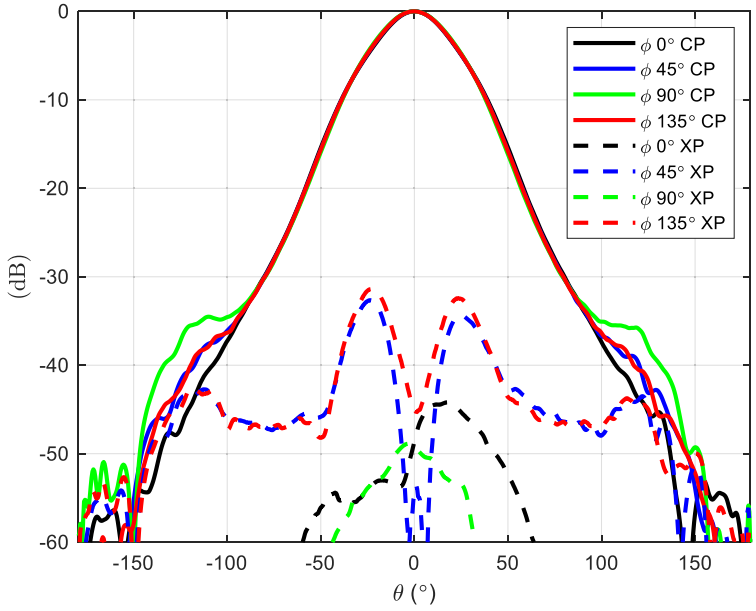


**Fig. 9.** Measurement of the normalized co-polar (solid line) and cross-polar (dash line) radiation patterns for the angles $0°, 45°, 90°$ and $135°$, for the vertical polarization at center frequency of 14.5 GHz.

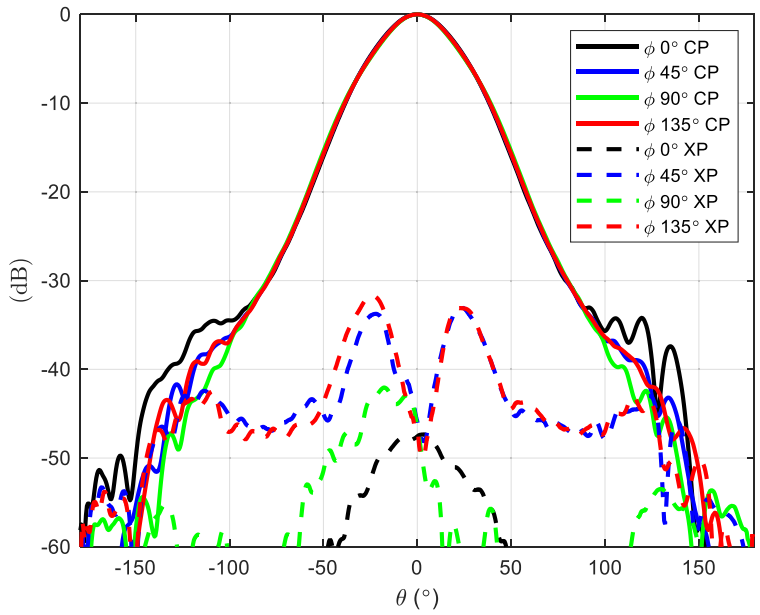


**Fig. 10.** Measurement of the normalized co-polar (solid line) and cross-polar (dash line) radiation patterns for the angles $0°, 45°, 90°$ and $135°$, for the horizontal polarization at center frequency of 14.5 GHz.

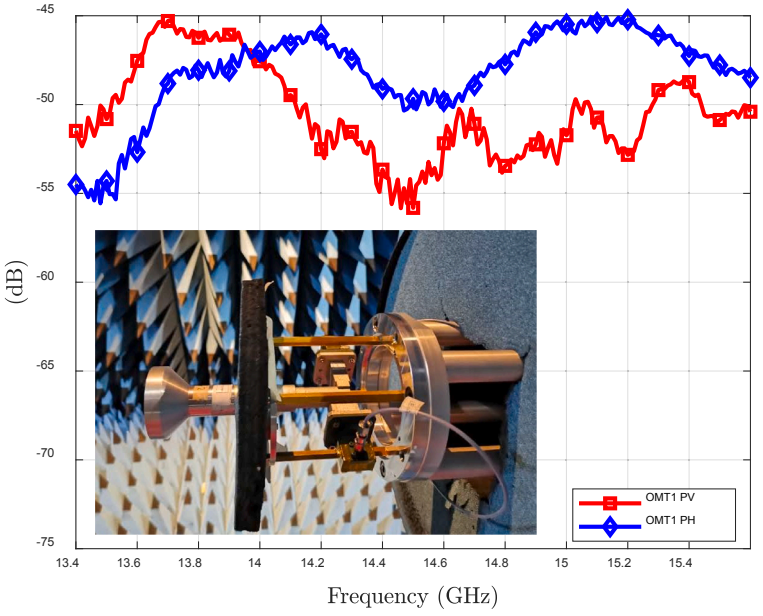


**Fig. 11.** Measured cross-polarization for the vertical (VP) and horizontal (HP) polarizations for $\theta = 0°, \phi = 0°$. In the inset, a photograph of the OMT positioned in the anechoic chamber to measure the radiation patterns and cross-polarization.

**Table 1**
Comparison between the proposed OMT and other asymmetric OMTs in the state of the art.

| OMT | Normalized size at $\lambda_0]_{f_{min}}$ | Return loss (dB) | Insertion loss (dB) | Isolation (dB) | Frequency band (GHz) | Fractional bandwidth (%) | Manufacturing technology |
|---|---|---|---|---|---|---|---|
| [34]-2011 | - | 20 | – | 45 | 23–28 | 19.6 | CNC milling |
| [37]-2018 | – | 22.5 | – | 65 | 8.5–9.6 | 12 | CNC milling |
| [38]-2020 | – | 15 | – | 45 | 21.5–25.5 | 17.8 | CNC milling |
| [26]-2018 | $3.7 \times 1.2 \times 6.5$ | 25 | 0.22 | 40 | 28–33 | 15.4 | SLM AlSi10Mg |
| [29]-2017 | – | 22 | 0.2 | 35 | K | 8 | SLM AlSi10Mg |
| [24]-2016 | – | 15 | 2.5 | – | 17–22;27–31 | 25.6;13.8 | SL Polymer + copper |
| [31]-2020 | $1.3 \times 1.2 \times 0.7$ | 16 | 0.34 | 40 | 2.7–3.2 | 16.7 | SLM AlSi10Mg |
| This work | $3.7 \times 3.4 \times 2.5$ | 20 | 0.18 | 45 | 13.4–15.6 | 15.2 | SLM AlSi10Mg |

## 4. Conclusion

This paper presents an ortho-mode transducer specifically conceived for metallic additive manufacturing in a single-block by selective laser melting (SLM). A short-circuited T-junction is the common circular waveguide where the two rectangular waveguides ports are connected with a relative angle of 180°. Operating in Ku-band from 13.4 to 15.6 GHz (15.2%), the measured return loss level is higher than 20 dB, the insertion loss is lower than 0.18 dB and the isolation is higher than 45 dB. The cross-polar radiation is lower than −45 dB for both polarizations.

These results are obtained simplifying the structure, reducing the number of matching elements for both polarizations and by means of an strong interaction between the electric and the mechanic engineer in charge of the manufacturing. Besides, a trade-off between the response of both polarizations in the optimization process is mandatory to obtain the very competitive reported experimental results, which can be required at incoming satellite systems. Finally, the suitability of the SLM technology for this kind of device has been shown, providing the advantages of a) lower cost (850$ per single part) than classic Computer Numerical Control (CNC) technology, and b) single-block manufacturing for reducing the number of parts and improving losses and power handling capability.

## Declaration of Competing Interest

The authors declare that they have no known competing financial interests or personal relationships that could have appeared to influence the work reported in this paper.

## Acknowledgment

This work was supported by the Spanish Government under grant TEC2016-76070-C3-1/2-R (Agencia Estatal de Investigación, Fondo Europeo de Desarrollo Regional: AEI/FEDER, UE).

The authors would like to thank IDONIAL Centro Tecnológico, the diligence in the manufacturing process.

## References

[1] Uher J, Bornemann J, Rosenberg U. Waveguide Components for Antenna Feed Systems: Theory and CAD. Boston, MA, USA: Artech House; 1993.
[2] Pelosi G, Nesti R, Gentili GG. Orthomode transducers, Encyclopedia of RF and Microwave Engineering. New York, NY, USA: Wiley; 2005.
[3] Bøifot AM. Classification of ortho-mode transducers. Eur Trans Telecomm Rel Techn 1991;2(5):503–10.
[4] Rao SK. Advanced antenna technologies for satellite communications payloads. IEEE Trans Antennas Propag 2015;63(4):1205–17.
[5] Rao S, Kralovec J. Compact high-performance reflector-antenna feeds and feed networks for space applications [antenna applications]. IEEE Antennas Propag Mag 2010;52(4):210–7.
[6] Villiers DILD, Meyer P, Palmer KD. Broadband offset quad-ridged waveguide orthomode transducer. Electron Lett 2009;45(1):60–2.
[7] Dunning A, Srikanth S, Kerr AR. A simple orthomode transducer for centimeter to submillimeter wavelengths. In: Proc. 20th Int. Symp. Space Terahertz Technol.; 2009. p. 1–4.
[8] Navarrini A, Groppi C, Chattopadhyay G. A waveguide orthomode transducer for 385–500 GHz. In: Proc. 21th Int. Space THz Technol. Symp.; 2010. p. 23–5.
[9] Coutts GM. Octave bandwidth orthomode transducers for the expanded very large array. IEEE Trans Antennas Propag 2011;59(6):1910–7.
[10] Coutts GM. Wideband diagonal quadruple-ridge orthomode transducer for circular polarization detection. IEEE Trans Antennas Propag 2011;59(6):1902–9.
[11] Ruiz-Cruz JA, Montejo-Garai JR, Leal-Sevillano CA, Rebollar JM. Orthomode Transducers With Folded Double-Symmetry Junctions for Broadband and Compact Antenna Feeds. IEEE Trans Antennas Propag 2018;66(3):1160–8. https://doi.org/10.1109/TAP.2018.2794364.
[12] Mishra PK, et al. High-Throughput Satellite Characterization: Spot beam payload characterization of high-throughput satellites in a compact antenna test facility. IEEE Antennas Propag Mag 2019;61(5):69–76. https://doi.org/10.1109/MAP.2019.2932314.
[13] Pultarova T. Mega-constellations: Will they bridge [Space Communications]. Eng Technol 2018;13(1):66–9. https://doi.org/10.1049/et.2018.0108.
[14] Gibson I, Rosen DW, Stucker B. Additive Manufacturing Technologies: Rapid Prototyping to Direct Digital Manufacturing. New York, NY, USA: Springer-Verlag; 2010.
[15] Barnatt C. 3D printing. 2nd ed. Createspace Independent Pub; 2014.
[16] Additive manufacturing-General principles-Terminology. ISO/ASTM 52900:2015 (ASTM F2792); 2015.
[17] Montejo-Garai JR, Saracho-Pantoja IO, Leal-Sevillano C, Ruiz-Cruz JA, Rebollar JM. Design of microwave waveguide devices for space and ground application implemented by additive manufacturing. In: 2015 International Conference on Electromagnetics in Advanced Applications (ICEAA); 2015. p. 325–8. https://doi.org/10.1109/ICEAA.2015.7297128.
[18] Sorrentino R, Martin-Iglesias P, Peverini OA, Weller TM. Additive Manufacturing of Radio-Frequency Components [Scanning the Issue]. Proc IEEE 2017;105(4):589–92. https://doi.org/10.1109/JPROC.2017.2670298.
[19] Kyovtorov V, Georgiev I, Margenov S, Stoychev D, Oliveri F, Tarchi D. New antenna design approach – 3D polymer printing and metallization. experimental test at 14–18GHz. AEU Int J Electron Commun 2017;73:119–28. https://doi.org/10.1016/j.aeue.2016.12.017.
[20] Peverini OA, et al. Selective Laser Melting Manufacturing of Microwave Waveguide Devices. Proc IEEE 2017;105(4):620–31. https://doi.org/10.1109/JPROC.2016.2620148. April.
[21] T. Tomura, Y. Miura, M. Zhang, J. Hirokawa, M. Ando. A 45° Linearly Polarized Hollow-Waveguide Corporate-Feed Slot Array Antenna in the 60-GHz Band, IEEE Transactions on Antennas and Propagation, 60(8), 3640–3646, doi: 10.1109/TAP.2012.2201094.
[22] Garcia-Marin E, Masa-Campos J-L, Sanchez-Olivares P. Diffusion-bonded W-band monopulse array antenna for space debris radar. AEU Int J Electron Commun 2020;116:153061. https://doi.org/10.1016/j.aeue.2019.153061.
[23] Bhutani A, et al. 3D metal printed Ku/Ka Band modified turnstile junction Orthomode Transducer. Proc. 2016 Asia-Pacific Microwave Conference (APMC), New Delhi 2016:1–4. https://doi.org/10.1109/APMC.2016.7931276.
[24] Shang X, Klasmann P, Lancaster MJ. A compact Ka-band waveguide orthomode transducer fabricated by 3-D printing. Proc. 2016 46th European Microwave Conference (EuMC), London 2016:365–8. https://doi.org/10.1109/EuMC.2016.7824354.
[25] Addamo G, Peverini OA, Virone G, Paonessa F, Manfredi D, Calignano F. 3D Printing of Ka band Orthomode Transducers. Proc.2018 IEEE MTT-S International

Microwave Workshop Series on Advanced Materials and Processes for RF and THz Applications (IMWS-AMP), Ann Arbor, MI 2018:1–3. https://doi.org/10.1109/IMWS-AMP.2018.8457143.

[26] Addamo G, et al. Additive Manufacturing of Ka-Band Dual-Polarization Waveguide Components. IEEE Trans Microw Theory Techn 2018;66(8):3589–96. https://doi.org/10.1109/TMTT.2018.2854187. Aug.

[27] Addamo G, et al. Electromagnetic and mechanical analyses of a 3D-printed ka-band integrated twist and orthomode transducer. Proc. 2019 IEEE MTT-S International Microwave Workshop Series on Advanced Materials and Processes for RF and THz Applications (IMWS-AMP), Bochum, Germany 2019:31–3. https://doi.org/10.1109/IMWS-AMP.2019.8880125.

[28] Abdelaal MA, Kishk AA. Ka-Band 3-D-Printed Wideband Groove Gap Waveguide Orthomode Transducer. IEEE Trans Microw Theory Techn 2019;67(8):3361–9. https://doi.org/10.1109/TMTT.2019.2919630.

[29] Yukawa H, Ushijima Y, Abe M, Yoneda N, Miyazaki M. A metal 3D-printed T-junction OMT with an offset stepped post. Proc. 2017 47th European Microwave Conference (EuMC), Nuremberg 2017:444–7. https://doi.org/10.23919/EuMC.2017.8230885.

[30] Feng B, Tu Y, Chen J, Chung KL, Sun S. High-performance dual circularly-polarized antenna arrays using 3D printing for 5G millimetre-wave communications. AEU Int J Electron Commun 2021;130:153569. https://doi.org/10.1016/j.aeue.2020.153569.

[31] A. Liu, J. Lu and S.M. Sow, A Compact 3-D Printed Asymmetric Orthogonal Mode Transducer, IEEE Trans. Antennas Propag., doi: 10.1109/TAP.2020.3044375 (in-press).

[32] Yoneda N, Miyazaki M, Tanaka M, Nakaguro H. Design of compact-size high isolation branching OMT by the mode-matching technique. Proc.1996 26th European Microwave Conference, Prague, Czech Republic 1996:848–51. https://doi.org/10.1109/EUMA.1996.337709.

[33] U. Rosenberg and R. Beyer, Very compact ortho-mode transducer suited for integrated feed system solutions, in Proc. 2011 IEEE International Conference on Microwaves, Communications, Antennas and Electronic Systems (COMCAS 2011), Tel Aviv, 2011, pp. 1–3, doi: 10.1109/COMCAS.2011.6105924.

[34] Rosenberg U, Beyer R. Compact T-junction orthomode transducer facilitates easy integration and low cost production. Proc. 2011 41st European Microwave Conference, Manchester 2011:663–6. https://doi.org/10.23919/EuMC.2011.6101784.

[35] CST Microwave Studio; November 2020. https://www.3ds.com/products-services/simulia/products/cst-studio-suite/.

[36] Montejo-Garai JR, Ruiz-Cruz JA, Rebollar JM. Evaluation of Additive Manufacturing Techniques Applied to a Waveguide Mode Transducer. IEEE Trans Compon Packag Manuf Technol 2020;10(5):887–94. https://doi.org/10.1109/TCPMT.2020.2982735.

[37] Abdelaal MA, Shams SI, Kishk AA. Asymmetric Compact OMT for X-Band SAR Applications. IEEE Trans Microw Theory Techn 2018;66(4):1856–63.

[38] Wu Q, Fan C, Yang Y, Shi X. Ultra-compact taper branching orthomode transducer. Int J RF Microw Comput Aided Eng 2020;30(e22215). https://doi.org/10.1002/mmce.22215.